


Article

Thermodynamic Analysis and Experimental Investigation of Al and F Removal from Sulfuric Acid Leachate of Spent LiFePO₄ Battery Powder

Yafei Jie ¹, Shenghai Yang ^{1,2}, Pengfei Shi ¹, Di Chang ¹, Gang Fang ¹, Caixuan Mo ¹, Jiang Ding ¹, Zhiqiang Liu ^{3,4}, Yanqing Lai ^{1,2} and Yongming Chen ^{1,2,*} 

¹ School of Metallurgy and Environment, Central South University, Changsha 410083, China; yafeijie1221@126.com (Y.J.); yangsh@mail.csu.edu.cn (S.Y.); 183512165@csu.edu.cn (P.S.); cd203501005@csu.edu.cn (D.C.); gang.fang@csu.edu.cn (G.F.); mocx1101@csu.edu.cn (C.M.); 0501170314@csu.edu.cn (J.D.); laiyanning@csu.edu.cn (Y.L.)

² Hunan Provincial Key Laboratory of Nonferrous Value-added Metallurgy, Changsha 410083, China

³ Institute of Rare Metals, Guangdong Academy of Science, Guangzhou 510651, China; Lzqgd168@126.com

⁴ State Key Laboratory of Rare Metals Separation and Comprehensive Utilization, Guangzhou 510651, China

* Correspondence: csuchenyongming@163.com; Tel.: +86-186-8468-5548

Abstract: The co-precipitation thermodynamics of the Li⁺-Fe²⁺/Fe³⁺-Al³⁺-F⁻-SO₄²⁻-PO₄³⁻-H₂O system at 298 K is studied, aiming to understand the precipitation characteristics. Based on the principle of simultaneous equilibrium and the mass action law, the missing *K_{sp}* values of AlF₃ and FeF₃ were estimated. The results of thermodynamic calculation demonstrate that Al³⁺ and F⁻ in the sulfuric acid leachate could be preferentially precipitated in the form of AlPO₄ and FeF₃ by the precise adjustment of the final pH value. Only a small amount of P and Fe was lost by the precipitation of Fe₃(PO₄)₂·8H₂O, FePO₄, and Fe(OH)₃ during the purification process. Controlling the oxidation of ferrous ions effectively is of critical significance for the loss reduction of P and Fe. Precipitation experiments at different pH value indicated that the concentration of Al³⁺ and F⁻ in the leachate decreased as the final pH value rose from 3.05 to 3.90. When the final pH value was around 3.75, aluminum and fluoride ion impurities could be deeply purified, and the loss rate of phosphate ions and iron ions could be reduced as much as possible. Relevant research results can provide theoretical guidance for the purification of leachate in the wet recycling process of lithium-ion batteries.

Keywords: spent LiFePO₄ battery; sulfuric acid leachate purification; co-precipitation thermodynamics; aluminum precipitation; fluorine removal



Citation: Jie, Y.; Yang, S.; Shi, P.; Chang, D.; Fang, G.; Mo, C.; Ding, J.; Liu, Z.; Lai, Y.; Chen, Y. Thermodynamic Analysis and Experimental Investigation of Al and F Removal from Sulfuric Acid Leachate of Spent LiFePO₄ Battery Powder. *Metals* **2021**, *11*, 1641. <https://doi.org/10.3390/met11101641>

Academic Editors: Minkyu Paek, Jean François Blais and Hongyeun Kim

Received: 5 September 2021

Accepted: 12 October 2021

Published: 15 October 2021

Publisher's Note: MDPI stays neutral with regard to jurisdictional claims in published maps and institutional affiliations.



Copyright: © 2021 by the authors. Licensee MDPI, Basel, Switzerland. This article is an open access article distributed under the terms and conditions of the Creative Commons Attribution (CC BY) license (<https://creativecommons.org/licenses/by/4.0/>).

1. Introduction

Greenhouse gas emissions are severely aggravating global climate change, and thus all countries should formulate national policies to achieve zero carbon emissions [1,2]. China, for instance, has pledged to peak nationwide CO₂ emissions by 2030 and achieve carbon neutrality by 2060 [3,4]. Aimed at this goal, the zero-carbon industry represented by clean and renewable energy is facing a critical moment of accelerated development [5]. In the past decade, China has become the world's largest market of new energy vehicles (EV) as its EV stock reached 3,810,000 in 2019, nearly half of the global stock [6]. Given that the service life of power batteries is approximately 5–8 years, it is predicted that the cumulative decommissioning of powder batteries in China will reach 90.5 GWh from 2020 to 2022, of which spent LiFePO₄ batteries will account for 53.8% (48.7 GWh) [7].

Compared with traditional fuel vehicles, EV power battery systems use mineral resources such as lithium, cobalt, nickel, manganese, copper, aluminum, iron, phosphorus, and graphite [8]. Recycling valuable metal resources from discarded lithium batteries is the key to the sustainable development of the EV industry. On the other hand, if not professionally treated, potentially toxic components inside them would be directly disposed of

in the environment, causing serious damage to both humans and the environment [9–11]. Processes of dealing with spent LiFePO_4 batteries are the direct regeneration process and the hydrometallurgical method [12]. Although the direct regeneration process is relatively simple and inexpensive, the long-term performance of repaired electrode materials could hardly meet the standard of power battery materials [13]. The hydrometallurgical process is the mainstream technology for lithium iron phosphate batteries treatment in Chinese recycling enterprises because of its low energy consumption, high product purity, and wide adaptability of raw materials. This process mainly involves pretreatment, leaching (selective leaching of Li or simultaneous leaching of Fe and Li), purification, and preparation of battery materials. In the leaching process, mineral acids (H_2SO_4 [14–17], HCl [14,18,19], HNO_3 [14], H_3PO_4 [14,20–23]) and organic acids (oxalic acid [14,24,25], citric acid [14], acetic acid [14], methyl sulfonic acid [26], and *p*-toluene sulfonic acid [26]) are used as the leaching agent to dissolve the target metal in spent LiFePO_4 battery powder. Among them, H_2SO_4 is widely used as a leaching agent by lithium battery recycling companies due to its low price, easy fabrication, and strong acidity. Various impurity ions, such as Al, Cu, and F, will inevitably enter the leachate and finally affect the physicochemical properties of regenerated electrode materials. Current research on the purification process of leachate largely focuses on spent LiCoO_2 and ternary batteries; by contrast, there are few reports on the purification of acid leachate of the spent LiFePO_4 battery. At present, the purification process of leachate includes solvent extraction, ion exchange and chemical precipitation [27,28]. Solvent extraction and ion exchange can achieve deep and stable removal of impurity elements, but they also have disadvantages such as high operating costs and strict control requirements. According to the type of sediment, the purification process of chemical precipitation can be divided into various methods, such as hydrolyzation–precipitation [29–31], sulfide precipitation, halide precipitation [32], and double salt precipitation [33]. Pagnanelli et al. [29] used the chemical precipitation to preliminarily remove Cu, Fe, Ni, Mn and Al impurities from the leach liquor of LiCoO_2 electrodic powder. The results showed that iron was fully removed when the pH value increased to 3.8, but other metals were only partially removed. The increasing pH determined the abatement of metal impurities, but simultaneously the loss of Co. Joo et al. [30] achieved effective removal of impurities including Al, Fe and Cu in pre-treated leach liquors of ternary cathode material by precipitation at pH 4.8 adjusted by the addition of 4 M NaOH. Kang et al. [31] removed over 99% Fe, Cu and Al in their hydroxides form by adjusting the pH of leach liquor to 6.5. Weng et al. [32] used Na_2S as a precipitator to effectively remove impurity copper ions in the form of CuS precipitation. Although the chemical precipitation method is easy to operate and has a high removal efficiency, it is generally accompanied by the loss of valuable metals. Owing to the complex composition of the leachate and the strict impurity limits for electrode materials, the combined process of chemical precipitation and organic solvent extraction is usually required to achieve deep and stable removal of impurities.

In this paper, sulfuric acid solution commonly used by lithium battery recycling companies is used as the leaching agent to treat spent LiFePO_4 battery powder, the leachate contains various cations, such as Li^+ , Fe^{2+} , Fe^{3+} , Al^{3+} and several anions, such as F^- , SO_4^{2-} , and PO_4^{3-} . In the process of chemical precipitation or solvent extraction to remove aluminum and fluorine, ferric iron ions tend to preferentially enter the separated phase, resulting in the loss of valuable elements and increased reagent consumption. In this study, on the basis of the simultaneous equilibrium principle and mass action law, the co-precipitation thermodynamics of the $\text{Li}^+ - \text{Fe}^{2+} / \text{Fe}^{3+} - \text{Al}^{3+} - \text{F}^- - \text{SO}_4^{2-} - \text{PO}_4^{3-} - \text{H}_2\text{O}$ system is simulated and calculated to reveal the evolution law of the total equilibrium concentration of Al, F, P, and Fe, and the phase composition of precipitates at different final pH values, aiming to understand the precipitation characteristics. In addition, to validate the feasibility of thermodynamic calculation, trisodium phosphate dodecahydrate was used as neutralizer and ascorbic acid as a reducing agent to control the final pH value of

sulfuric acid leachate within predetermined range in an inert atmosphere and monitor the changes of Al, F, P and Fe contents in the leachate.

2. Experimental

2.1. Materials

Spent LiFePO_4 cathode powder was provided by a battery recycling company (Nantong, China), and it was separated from aluminum foils by thermal treatment and screening. The composition of collected spent LiFePO_4 cathode powder, determined by inductively coupled plasma optical emission spectroscopy (ICP-OES, SPECTROBLUE SOP) after leaching with aqua regia, is shown in Table 1. The sulfuric acid leaching solution is prepared by the leaching reaction of spent LiFePO_4 cathode powder with 2.5 M H_2SO_4 under the conditions of S/L = 1/7, leaching temperature 75 °C, and leaching time of 2 h. Prior to the precipitation, a small amount of reductive iron powder was added to leachate to remove the copper ions by replacement. It should be noted that since reductive iron powder was used to remove the copper ion by replacement, the iron ions in the solution mainly existed in the form of Fe^{2+} . The concentrations of metal ions (Fe, Li, Cu, Al, Na, K, Ca, Mg) and non-metal ions (P, S, Si) in the sulfuric acid leachate were examined by ICP-OES. The F content of sulfuric acid leachate was obtained through the fluoride ion selective electrode method. The composition of sulfuric acid leachate is shown in Table 2. Aside from main elements P, Fe, Li, and S, the composition of the solution also contains a small amount of impurity elements such as Al, F, Na, K, Ca, Si and Mg. Ascorbic acid and trisodium phosphate dodecahydrate used in the experiments were of analytical grade. The purity of high-purity argon gas was 99.99%.

Table 1. Chemical composition of the spent LiFePO_4 cathode powder.

Elements	P	Fe	Li	Cu	Al	F
Wt.%	15.9	38.5	3.76	0.5	1.4	0.8

Table 2. Chemical composition of the sulfuric acid leachate.

Elements	P	Fe	Li	Cu	Al	F
mg/L	22785.0	56320.0	5365.0	0.5	1999.0	1003.1
Elements	S	Na	K	Ca	Si	Mg
mg/L	84749.0	5.5	6.3	24.2	12.5	9.3

2.2. Methods

On the basis of the simultaneous equilibrium principle and mass action law, the co-precipitation thermodynamics of the $\text{Li}^+ - \text{Fe}^{2+} / \text{Fe}^{3+} - \text{Al}^{3+} - \text{F}^- - \text{SO}_4^{2-} - \text{PO}_4^{3-} - \text{H}_2\text{O}$ system is simulated. The calculation process based on the Newton-Raphson iteration method was carried out by using Microsoft Excel. Owing to the lack of complete data on the activity component in the solution, the molar concentration of each species was used to replace the activity coefficient in the thermodynamic calculation.

The schematic plot of the precipitation experiment set-up is illustrated in Figure 1. In the bench-scale precipitation experiments, 250 mL of the sulfuric acid leachate was poured into a three-necked flask immersed in a water bath at 25 °C. Afterward, 0.5 g of ascorbic acid, a reducing agent, was added to the leachate to reduce ferric ions. Simultaneously, high-purity argon was introduced to prevent the oxidation of ferrous ions. $\text{Na}_3\text{PO}_4 \cdot 12\text{H}_2\text{O}$ was added to the sulfuric acid leachate in real time to adjust the pH value of the system and keep it constant at a predetermined value. After the predetermined time, the liquid-solid separation of the feed solution was carried out, and then the composition of purified solution was analyzed by ICP-OES and the fluoride ion selective electrode method. The precipitate was vacuum dried at 60 °C for 24 h and then weighed and characterized.

The phase compositions of the precipitation were studied by X-ray diffraction (XRD, Rigaku D/max-2500, Rigaku Corporation, Tokyo, Japan) and Fourier transform infrared spectrometry (FT-IR, Nicolet 6700, Thermo Fisher Scientific, Waltham, USA). The elemental composition and chemical states on the surface of the electrode particles were detected by X-ray photoelectron spectroscopy (XPS, ESCALAB 250Xi, Thermo Fisher Scientific, Waltham, USA).

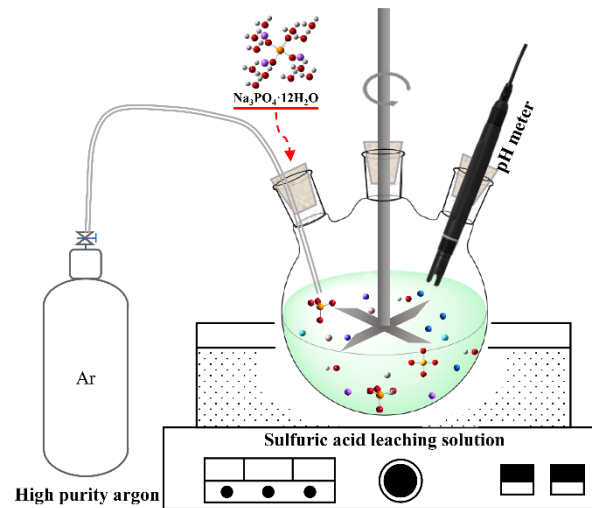


Figure 1. Schematic plot of the precipitation experiments set-up.

The removal rate of Al^{3+} and F^- as well as the loss rate of Fe during the purification process were computed by Equation (1).

$$R_i = \frac{C_{i_0} \times V_0 - C_{i_1} \times V_1}{C_{i_0} \times V_0} \times 100\% \quad (1)$$

where R_i (%) is the removal rate of Al^{3+} and F^- as well as the loss rate of Fe^{2+} , V_0 (mL) is the volume of sulfuric acid leachate, V_1 (mL) is the volume of purified solution, C_{i_0} (mg/L) is the concentration of Al^{3+} , F^- , and Fe^{2+} in the sulfuric acid leachate, and C_{i_1} (mg/L) is the concentration of Al^{3+} , F^- , and Fe^{2+} in the purified solution.

The loss rate of PO_4^{3-} in the purification process was calculated by Equation (2).

$$L_P = \frac{C_{p_0} \times V_0 - C_{p_1} \times V_1}{C_{p_0} \times V_0 + \frac{m_p \times 95}{380}} \times 100\% \quad (2)$$

where L_P (%) is the loss rate of PO_4^{3-} , V_0 (mL) is the volume of sulfuric acid leachate, V_1 (mL) is the volume of purified solution, C_{p_0} (mg/L) is the concentration of PO_4^{3-} in the sulfuric acid leachate, C_{p_1} (mg/L) is the concentration of PO_4^{3-} in the purified solution, and m_p (g) is the $\text{Na}_3\text{PO}_4 \cdot 12\text{H}_2\text{O}$ dosage.

3. Thermodynamic Data and Calculation Model

3.1. Ion Species and Their Thermodynamic Data

In the $\text{Li}^+ - \text{Fe}^{2+} / \text{Fe}^{3+} - \text{Al}^{3+} - \text{PO}_4^{3-} - \text{SO}_4^{2-} - \text{F}^- - \text{H}_2\text{O}$ system, the main species in the solution were assumed to be H^+ , OH^- , F^- , PO_4^{3-} , HPO_4^{2-} , H_2PO_4^- , H_3PO_4 , H_2SO_4 , HSO_4^- , Fe^{2+} , SO_4^{2-} , $\text{FeSO}_4(\text{aq})$, FeOH^+ , $\text{Fe}(\text{OH})_2(\text{aq})$, $\text{Fe}(\text{OH})_3^-$, $\text{Fe}(\text{OH})_4^{2-}$, $\text{FeHPO}_4(\text{aq})$, $\text{FeH}_2\text{PO}_4^+$, FeF^+ , Fe^{3+} , FeSO_4^+ , $\text{Fe}(\text{SO}_4)_2^-$, FeOH^{2+} , $\text{Fe}(\text{OH})_2^+$, $\text{Fe}(\text{OH})_4^-$, $\text{Fe}_2(\text{OH})_2^{4+}$, $\text{Fe}_3(\text{OH})_4^{5+}$, FeHPO_4^+ , $\text{FeH}_2\text{PO}_4^{2+}$, FeF^{2+} , FeF_2^+ , $\text{FeF}_3(\text{aq})$, Li^+ , LiSO_4^- , $\text{Li}(\text{OH})(\text{aq})$, LiHPO_4^- , $\text{Al}(\text{OH})_2^+$, $\text{Al}(\text{OH})_2^+$, $\text{Al}(\text{OH})_3(\text{aq})$, $\text{Al}(\text{OH})_4^-$, $\text{Al}_2(\text{OH})_2^{4+}$, $\text{Al}_3(\text{OH})_4^{5+}$, AlF^{2+} , AlF_2^+ , $\text{AlF}_3(\text{aq})$, AlF_4^- , AlF_5^{2-} , and AlF_6^{3-} . The reaction equations among these species and their equilibrium constant (K) are shown in Table 3.

Table 3. Thermodynamic equilibrium equations and their equilibrium constants in the $\text{Li}^+ - \text{Fe}^{2+} / \text{Fe}^{3+} - \text{Al}^{3+} - \text{PO}_4^{3-} - \text{SO}_4^{2-} - \text{F}^- - \text{H}_2\text{O}$ system (298 K) [34–36].

Equation No.	Reaction	log K	Chemical Equilibrium Constant Relationship
(3)	$\text{H}_2\text{O} = \text{H}^+ + \text{OH}^-$	−14	$[\text{H}_2\text{O}] = [\text{H}^+] \times [\text{OH}^-] \times 10^{14}$
(4)	$\text{H}_3\text{PO}_4 = \text{H}^+ + \text{H}_2\text{PO}_4^-$	−2.04	$[\text{H}_3\text{PO}_4] = [\text{H}^+] \times [\text{H}_2\text{PO}_4^-] \times 10^{2.04}$
(5)	$\text{H}_2\text{PO}_4^- = \text{H}^+ + \text{HPO}_4^{2-}$	−7.2	$[\text{H}_2\text{PO}_4^-] = [\text{H}^+] \times [\text{HPO}_4^{2-}] \times 10^{7.2}$
(6)	$\text{HPO}_4^{2-} = \text{H}^+ + \text{PO}_4^{3-}$	−12.36	$[\text{HPO}_4^{2-}] = [\text{H}^+] \times [\text{PO}_4^{3-}] \times 10^{12.36}$
(7)	$\text{H}_2\text{SO}_4 = \text{HSO}_4^- + \text{H}^+$	3	$[\text{H}_2\text{SO}_4] = [\text{HSO}_4^-] \times [\text{H}^+] \times 10^{-3}$
(8)	$\text{HSO}_4^- = \text{SO}_4^{2-} + \text{H}^+$	−1.99	$[\text{HSO}_4^-] = [\text{SO}_4^{2-}] \times [\text{H}^+] \times 10^{1.99}$
(9)	$\text{FeSO}_{4(\text{aq})} = \text{SO}_4^{2-} + \text{Fe}^{2+}$	−2.2	$[\text{FeSO}_{4(\text{aq})}] = [\text{SO}_4^{2-}] \times [\text{Fe}^{2+}] \times 10^{2.2}$
(10)	$\text{FeOH}^+ = \text{Fe}^{2+} + \text{OH}^-$	−4.5	$[\text{FeOH}^+] = [\text{Fe}^{2+}] \times [\text{OH}^-] \times 10^{4.5}$
(11)	$\text{Fe}(\text{OH})_{2(\text{aq})} = \text{Fe}^{2+} + 2\text{OH}^-$	−7.4	$[\text{Fe}(\text{OH})_{2(\text{aq})}] = [\text{Fe}^{2+}] \times [\text{OH}^-]^2 \times 10^{7.4}$
(12)	$\text{Fe}(\text{OH})_3^- = \text{Fe}^{2+} + 3\text{OH}^-$	−10.0	$[\text{Fe}(\text{OH})_3^-] = [\text{Fe}^{2+}] \times [\text{OH}^-]^3 \times 10^{10.0}$
(13)	$\text{Fe}(\text{OH})_4^{2-} = \text{Fe}^{2+} + 4\text{OH}^-$	−9.6	$[\text{Fe}(\text{OH})_4^{2-}] = [\text{Fe}^{2+}] \times [\text{OH}^-]^4 \times 10^{9.6}$
(14)	$\text{FeHPO}_{4(\text{aq})} = \text{Fe}^{2+} + \text{HPO}_4^{2-}$	−3.6	$[\text{FeHPO}_{4(\text{aq})}] = [\text{Fe}^{2+}] \times [\text{HPO}_4^{2-}] \times 10^{3.6}$
(15)	$\text{FeH}_2\text{PO}_4^+ = \text{Fe}^{2+} + \text{H}_2\text{PO}_4^-$	−2.7	$[\text{FeH}_2\text{PO}_4^+] = [\text{Fe}^{2+}] \times [\text{H}_2\text{PO}_4^-] \times 10^{2.7}$
(16)	$\text{FeF}^+ = \text{Fe}^{2+} + \text{F}^-$	−0.8	$[\text{FeF}^+] = [\text{Fe}^{2+}] \times [\text{F}^-] \times 10^{0.8}$
(17)	$\text{FeSO}_4^+ = \text{Fe}^{3+} + \text{SO}_4^{2-}$	−4.04	$[\text{FeSO}_4^+] = [\text{Fe}^{3+}] \times [\text{SO}_4^{2-}] \times 10^{4.04}$
(18)	$\text{Fe}(\text{SO}_4)_2^- = \text{Fe}^{3+} + 2\text{SO}_4^{2-}$	−5.38	$[\text{Fe}(\text{SO}_4)_2^-] = [\text{Fe}^{3+}] \times [\text{SO}_4^{2-}]^2 \times 10^{5.38}$
(19)	$\text{FeOH}^{2+} = \text{Fe}^{3+} + \text{OH}^-$	−11.81	$[\text{FeOH}^{2+}] = [\text{Fe}^{3+}] \times [\text{OH}^-] \times 10^{11.81}$
(20)	$\text{Fe}(\text{OH})_2^+ = \text{Fe}^{3+} + 2\text{OH}^-$	−22.3	$[\text{Fe}(\text{OH})_2^+] = [\text{Fe}^{3+}] \times [\text{OH}^-]^2 \times 10^{22.3}$
(21)	$\text{Fe}(\text{OH})_4^- = \text{Fe}^{3+} + 4\text{OH}^-$	−34.4	$[\text{Fe}(\text{OH})_4^-] = [\text{Fe}^{3+}] \times [\text{OH}^-]^4 \times 10^{34.4}$
(22)	$\text{Fe}_2(\text{OH})_2^{4+} = 2\text{Fe}^{3+} + 2\text{OH}^-$	−25.1	$[\text{Fe}_2(\text{OH})_2^{4+}] = [\text{Fe}^{3+}]^2 \times [\text{OH}^-]^2 \times 10^{25.1}$
(23)	$\text{Fe}_3(\text{OH})_4^{5+} = 3\text{Fe}^{3+} + 4\text{OH}^-$	−49.7	$[\text{Fe}_3(\text{OH})_4^{5+}] = [\text{Fe}^{3+}]^3 \times [\text{OH}^-]^4 \times 10^{49.7}$
(24)	$\text{FeHPO}_4^+ = \text{Fe}^{3+} + \text{HPO}_4^{2-}$	−8.30	$[\text{FeHPO}_4^+] = [\text{Fe}^{3+}] \times [\text{HPO}_4^{2-}] \times 10^{8.30}$
(25)	$\text{FeH}_2\text{PO}_4^{2+} = \text{Fe}^{3+} + \text{H}_2\text{PO}_4^-$	−3.47	$[\text{FeH}_2\text{PO}_4^{2+}] = [\text{Fe}^{3+}] \times [\text{H}_2\text{PO}_4^-] \times 10^{3.47}$
(26)	$\text{FeF}^{2+} = \text{Fe}^{3+} + \text{F}^-$	−6.0	$[\text{FeF}^{2+}] = [\text{Fe}^{3+}] \times [\text{F}^-] \times 10^{6.0}$
(27)	$\text{FeF}_2^+ = \text{Fe}^{3+} + 2\text{F}^-$	−9.07	$[\text{FeF}_2^+] = [\text{Fe}^{3+}] \times [\text{F}^-]^2 \times 10^{9.07}$
(28)	$\text{FeF}_{3(\text{aq})} = \text{Fe}^{3+} + 3\text{F}^-$	−12.1	$[\text{FeF}_{3(\text{aq})}] = [\text{Fe}^{3+}] \times [\text{F}^-]^3 \times 10^{12.1}$
(29)	$\text{Li}(\text{OH})_{(\text{aq})} = \text{Li}^+ + \text{OH}^-$	−0.36	$[\text{Li}(\text{OH})_{(\text{aq})}] = [\text{Li}^+] \times [\text{OH}^-] \times 10^{0.36}$
(30)	$\text{LiSO}_4^- = \text{SO}_4^{2-} + \text{Li}^+$	−0.64	$[\text{LiSO}_4^-] = [\text{SO}_4^{2-}] \times [\text{Li}^+] \times 10^{0.64}$
(31)	$\text{LiHPO}_4^- = \text{Li}^+ + \text{HPO}_4^{2-}$	−0.72	$[\text{LiHPO}_4^-] = [\text{Li}^+] \times [\text{HPO}_4^{2-}] \times 10^{0.72}$
(32)	$\text{Al}(\text{OH})_2^+ = \text{Al}^{3+} + \text{OH}^-$	−9.01	$[\text{Al}(\text{OH})_2^+] = [\text{Al}^{3+}] \times [\text{OH}^-] \times 10^{9.01}$
(33)	$\text{Al}(\text{OH})_2^+ = \text{Al}^{3+} + 2\text{OH}^-$	−18.7	$[\text{Al}(\text{OH})_2^+] = [\text{Al}^{3+}] \times [\text{OH}^-]^2 \times 10^{18.7}$
(34)	$\text{Al}(\text{OH})_{3(\text{aq})} = \text{Al}^{3+} + 3\text{OH}^-$	−27.0	$[\text{Al}(\text{OH})_{3(\text{aq})}] = [\text{Al}^{3+}] \times [\text{OH}^-]^3 \times 10^{27.0}$
(35)	$\text{Al}(\text{OH})_4^- = \text{Al}^{3+} + 4\text{OH}^-$	−33.0	$[\text{Al}(\text{OH})_4^-] = [\text{Al}^{3+}] \times [\text{OH}^-]^4 \times 10^{33.0}$
(36)	$\text{Al}_2(\text{OH})_2^{4+} = 2\text{Al}^{3+} + 2\text{OH}^-$	−20.3	$[\text{Al}_2(\text{OH})_2^{4+}] = [\text{Al}^{3+}]^2 \times [\text{OH}^-]^2 \times 10^{20.3}$
(37)	$\text{Al}_3(\text{OH})_4^{5+} = 3\text{Al}^{3+} + 4\text{OH}^-$	−42.1	$[\text{Al}_3(\text{OH})_4^{5+}] = [\text{Al}^{3+}]^3 \times [\text{OH}^-]^4 \times 10^{42.1}$
(38)	$\text{AlF}^{2+} = \text{Al}^{3+} + \text{F}^-$	−6.09	$[\text{AlF}^{2+}] = [\text{Al}^{3+}] \times [\text{F}^-] \times 10^{6.09}$
(39)	$\text{AlF}_2^+ = \text{Al}^{3+} + 2\text{F}^-$	−11.12	$[\text{AlF}_2^+] = [\text{Al}^{3+}] \times [\text{F}^-]^2 \times 10^{11.12}$
(40)	$\text{AlF}_{3(\text{aq})} = \text{Al}^{3+} + 3\text{F}^-$	−15	$[\text{AlF}_{3(\text{aq})}] = [\text{Al}^{3+}] \times [\text{F}^-]^3 \times 10^{15}$
(41)	$\text{AlF}_4^- = \text{Al}^{3+} + 4\text{F}^-$	−18	$[\text{AlF}_4^-] = [\text{Al}^{3+}] \times [\text{F}^-]^4 \times 10^{18}$
(42)	$\text{AlF}_5^{2-} = \text{Al}^{3+} + 5\text{F}^-$	−19.4	$[\text{AlF}_5^{2-}] = [\text{Al}^{3+}] \times [\text{F}^-]^5 \times 10^{19.4}$
(43)	$\text{AlF}_6^{3-} = \text{Al}^{3+} + 6\text{F}^-$	−19.8	$[\text{AlF}_6^{3-}] = [\text{Al}^{3+}] \times [\text{F}^-]^6 \times 10^{19.8}$

3.2. Solid Species and Their Thermodynamic Data

In the $\text{Li}^+ - \text{Fe}^{2+} / \text{Fe}^{3+} - \text{Al}^{3+} - \text{PO}_4^{3-} - \text{SO}_4^{2-} - \text{F}^- - \text{H}_2\text{O}$ system, $\text{Fe}_3(\text{PO}_4)_2 \cdot 8\text{H}_2\text{O}$, $\text{FePO}_4 \cdot 2\text{H}_2\text{O}$, $\text{Al}(\text{OH})_3$, AlPO_4 , Li_3PO_4 , AlF_3 , FeF_3 , FeF_2 , LiF , $\text{Fe}(\text{OH})_2$, and $\text{Fe}(\text{OH})_3$ precipitations formed as the pH value and ion concentration in the solution changed. The solubility product constants K_{sp} of AlF_3 and FeF_3 , as well as their thermodynamic data $\Delta_f G_i^\theta$ and $\Delta_f S_i^\theta$, have not been reported before in the literature. In this paper, the K_{sp} value of AlF_3 and FeF_3 was estimated according to their solubility and the equilibrium model of gradual dissociation.

3.2.1. Calculation of K_{sp} value of AlF_3

Assuming that a certain amount of AlF_3 was added to deionized water, when AlF_3 reached dissolution equilibrium, the main species in the solution and their equilibrium equations can be shown in Equations (38)–(43) in Table 2.

According to the simultaneous equilibrium principle and mass action law, the mass balance equations of F and Al are given as follows:

$$[F]_T = [F^-] + [AlF^{2+}] + 2[AlF_2^+] + 3[AlF_3] + 4[AlF_4^-] + 5[AlF_5^{2-}] + 6[AlF_6^{3-}] \quad (44)$$

$$[Al]_T = [Al^{3+}] + [AlF^{2+}] + [AlF_2^+] + [AlF_3] + [AlF_4^-] + [AlF_5^{2-}] + [AlF_6^{3-}] \quad (45)$$

where $[F]_T$ and $[Al]_T$ are designated as the total concentration of F and Al in equilibrium conditions; $[Al^{3+}]$, $[F^-]$, $[AlF^{2+}]$, $[AlF_2^+]$, $[AlF_3]$, $[AlF_4^-]$, $[AlF_5^{2-}]$, and $[AlF_6^{3-}]$ are defined as the equilibrium concentration for each species in equilibrium conditions.

The chemical equilibrium constant relationship of Equations (38)–(43) in Table 1 is substituted into Equations (44) and (45) to obtain Equations (46) and (47).

$$[F]_T = [F^-] + [Al^{3+}] \times [F^-] \times 10^{6.09} + 2([Al^{3+}] \times [F^-]^2 \times 10^{11.12}) + 3([Al^{3+}] \times [F^-]^3 \times 10^{15}) + 4([Al^{3+}] \times [F^-]^4 \times 10^{18}) + 5([Al^{3+}] \times [F^-]^5 \times 10^{19.4}) + 6([Al^{3+}] \times [F^-]^6 \times 10^{19.8}) \quad (46)$$

$$[Al]_T = [Al^{3+}] + [Al^{3+}] \times [F^-] \times 10^{6.09} + [Al^{3+}] \times [F^-]^2 \times 10^{11.12} + [Al^{3+}] \times [F^-]^3 \times 10^{15} + [Al^{3+}] \times [F^-]^4 \times 10^{18} + [Al^{3+}] \times [F^-]^5 \times 10^{19.4} + [Al^{3+}] \times [F^-]^6 \times 10^{19.8} \quad (47)$$

According to the literature, the solubility of AlF_3 is 0.67 g/100 mL of water at 20 °C [34]. Below this temperature, when AlF_3 reached dissolution equilibrium, the $[F]_T$ and $[Al]_T$ values would be 0.239352 and 0.079784 mol/L, respectively. Combined with Equations (46) and (47), the $[F^-]$ and $[Al^{3+}]$ values were 3.965×10^{-4} mol/L and 9.43×10^{-7} mol/L when AlF_3 reached dissolution equilibrium.

The K_{sp} definition of $AlF_3(s)$ is shown in Equation (48). The K_{sp} value of $AlF_3(s)$ was calculated to be 4.53×10^{-17} .

$$K_{sp} = [F^-]^3 \times [Al^{3+}] \quad (48)$$

3.2.2. Calculation of K_{sp} value of FeF_3

Given that a certain amount of FeF_3 was added to deionized water, when FeF_3 reached dissolution equilibrium, the main species in the solution and their equilibrium equations can be shown in Equations (26)–(28) in Table 2.

On the basis of the simultaneous equilibrium principle and mass action law, the mass balance equations of F and Fe are given as follows:

$$[F]_T = [F^-] + [FeF^{2+}] + 2[FeF_2^+] + 3[FeF_3] \quad (49)$$

$$[Fe]_T = [Fe^{3+}] + [FeF^{2+}] + [FeF_2^+] + [FeF_3] \quad (50)$$

where $[F]_T$ and $[Fe]_T$ are designated as the total concentration of F and Fe in equilibrium conditions; $[Fe^{3+}]$, $[F^-]$, $[FeF^{2+}]$, $[FeF_2^+]$, and $[FeF_3]$ are defined as the equilibrium concentration for each species in equilibrium conditions.

The chemical equilibrium constant relationship of Equations (26)–(28) in Table 2 is substituted into Equations (49) and (50) to obtain Equations (51) and (52).

$$[F]_T = [F^-] + ([Fe^{3+}] \times [F^-] \times 10^{6.0}) + 2([Fe^{3+}] \times [F^-]^2 \times 10^{9.07}) + 3([Fe^{3+}] \times [F^-]^3 \times 10^{12.1}) \quad (51)$$

$$[Fe]_T = [Fe^{3+}] + [Fe^{3+}] \times [F^-] \times 10^{6.0} + [Fe^{3+}] \times [F^-]^2 \times 10^{9.07} + [Fe^{3+}] \times [F^-]^3 \times 10^{12.1} \quad (52)$$

According to the literature, the solubility of FeF_3 is 0.091 g/100 mL of water at 20 °C [34]. In this case, when FeF_3 reached dissolution equilibrium, the $[F]_T$ and $[Fe]_T$ values would be 0.024193503 and 0.008064501 mol/L, respectively. From Equations (51) and (52), the $[F^-]$ and $[Fe^{3+}]$ values were 7.52×10^{-6} mol/L and 8.51×10^{-10} mol/L when FeF_3 reached dissolution equilibrium.

The K_{sp} definition of $FeF_3(s)$ is presented in Equation (53). The K_{sp} value of $FeF_3(s)$ was calculated to be 3.623×10^{-25} .

$$K_{sp} = [F^-]^3 \times [Fe^{3+}] \quad (53)$$

3.2.3. Solid-State Reactions and Their Equilibrium Constant

The possible solid-state reactions among the species in the $Li^+-Fe^{2+}/Fe^{3+}-Al^{3+}-PO_4^{3-}-SO_4^{2-}-F^- -H_2O$ system and their corresponding equilibrium constants are listed in Table 4.

Table 4. Solid-state reactions and their equilibrium constant of $Li^+-Fe^{2+}/Fe^{3+}-Al^{3+}-PO_4^{3-}-SO_4^{2-}-F^- -H_2O$ system (298 K) [34–36].

Equation No.	Reaction	log K	Chemical Equilibrium Constant Relationship
(54)	$Fe_3(PO_4)_2 \cdot 8H_2O(s) = 3Fe^{2+} + 2PO_4^{3-} + 8H_2O$	−36.85	$[Fe^{2+}]^3 \times [PO_4^{3-}]^2 = 10^{-36.85}$
(55)	$FePO_4 \cdot 2H_2O(s) = Fe^{3+} + PO_4^{3-} + 2H_2O$	−15.0039	$[Fe^{3+}] \times [PO_4^{3-}] = 10^{-15.0039}$
(56)	$FePO_4(s) = Fe^{3+} + PO_4^{3-}$	−21.886	$[Fe^{3+}] \times [PO_4^{3-}] = 10^{-21.886}$
(57)	$Al(OH)_3 = Al^{3+} + 3OH^-$	−32.89	$[Al^{3+}] \times [OH^-]^3 = 10^{-32.89}$
(58)	$AlPO_4(s) = Al^{3+} + PO_4^{3-}$	−20.007	$[Al^{3+}] \times [PO_4^{3-}] = 10^{-20.007}$
(59)	$Li_3PO_4(s) = 3Li^+ + PO_4^{3-}$	−10.6253	$[Li^+]^3 \times [PO_4^{3-}] = 10^{-10.6253}$
(60)	$AlF_3(s) = Al^{3+} + 3F^-$	−16.3439	$[Al^{3+}] \times [F^-]^3 = 10^{-16.3439}$
(61)	$FeF_3(s) = Fe^{3+} + 3F^-$	−24.4409	$[Fe^{3+}] \times [F^-]^3 = 10^{-24.4409}$
(62)	$FeF_2(s) = Fe^{2+} + 2F^-$	−5.62709	$[Fe^{2+}] \times [F^-]^2 = 10^{-5.62709}$
(63)	$LiF(s) = Li^+ + F^-$	−2.77	$[Li^+] \times [F^-] = 10^{-2.77}$
(64)	$Fe(OH)_2(s) = Fe^{2+} + 2OH^-$	−16.31	$[Fe^{2+}] \times [OH^-]^2 = 10^{-16.31}$
(65)	$Fe(OH)_3(s) = Fe^{3+} + 3OH^-$	−38.8	$[Fe^{3+}] \times [OH^-]^3 = 10^{-38.8}$

3.3. Thermodynamic model of the $Li^+-Fe^{2+}-Al^{3+}-PO_4^{3-}-SO_4^{2-}-F^- -H_2O$ System

The soluble species in the $Li^+-Fe^{2+}-Al^{3+}-PO_4^{3-}-SO_4^{2-}-F^- -H_2O$ system and their equilibrium equations are shown in Equations (3)–(16) and (29)–(43) in Table 2, respectively. Via the simultaneous equilibrium principle, mass action law, and electroneutrality principle, Equations (66)–(72) were obtained.

$$[P]_T = [PO_4^{3-}] + [HPO_4^{2-}] + [H_2PO_4^-] + [H_3PO_4] + [LiHPO_4^-] + [FeHPO_4(aq)] + [FeH_2PO_4^+] \quad (66)$$

$$[Fe(II)]_T = [Fe^{2+}] + [FeSO_4(aq)] + [FeOH^+] + [Fe(OH)_2(aq)] + [Fe(OH)_3^-] + [Fe(OH)_4^{2-}] + [FeHPO_4(aq)] + [FeH_2PO_4^+] + [FeF^+] \quad (67)$$

$$[Li]_T = [Li^+] + [Li(OH)_{(aq)}] + [LiSO_4^-] + [LiHPO_4^-] \quad (68)$$

$$[S]_T = [SO_4^{2-}] + [H_2SO_4] + [HSO_4^-] + [FeSO_4(aq)] + [LiSO_4^-] \quad (69)$$

$$[Al]_T = [Al^{3+}] + [AlF^{2+}] + [AlF_2^+] + [AlF_3(aq)] + [AlF_4^-] + [AlF_5^{2-}] + [AlF_6^{3-}] + [Al(OH)_2^+] + [Al(OH)_3(aq)] + [Al(OH)_4^-] + 2[Al_2(OH)_2^{4+}] + 3[Al_3(OH)_4^{5+}] \quad (70)$$

$$[F]_T = [F^-] + [AlF^{2+}] + 2[AlF_2^+] + 3[AlF_3(aq)] + 4[AlF_4^-] + 5[AlF_5^{2-}] + 6[AlF_6^{3-}] + [FeF^+] \quad (71)$$

$$2[Fe^{2+}] + [FeOH^+] + [FeH_2PO_4^+] + [Li^+] + 3[Al^{3+}] + 2[Al(OH)_2^+] + [Al(OH)_3^-] + 4[Al_2(OH)_2^{4+}] + 5[Al_3(OH)_4^{5+}] + 2[AlF^{2+}] + [AlF_2^+] + [FeF^+] + [H^+] = [Fe(OH)_3^-] + 2[Fe(OH)_4^{2-}] + [H_2PO_4^-] + 2[HPO_4^{2-}] + 3[PO_4^{3-}] + [LiHPO_4^-] + [LiSO_4^-] + [Al(OH)_4^-] + [F^-] + [AlF_4^-] + 2[AlF_5^{2-}] + 3[AlF_6^{3-}] + 2[SO_4^{2-}] + [HSO_4^-] + [OH^-] \quad (72)$$

When a solid phase is formed in the system, each component in the solid phase stable region must satisfy not only Equations (3)–(16), (29)–(43), and (66)–(72) but also their corresponding constraint equations. The constraint equations for different solid phase stable regions are provided in Table 5.

Table 5. Constraint equations for different solid phase stable region.

Eq no.	Equation
(73)	$([\text{Fe(II)}]_{\text{O}} - [\text{Fe(II)}]_{\text{T}}) / ([\text{P}]_{\text{O}} - [\text{P}]_{\text{T}}) = 3/2$
(74)	$[\text{Fe}^{2+}]^3 \times [\text{PO}_4^{3-}]^2 = 10^{-36.85}$
(75)	$[\text{Al}]_{\text{O}} - [\text{Al}]_{\text{T}} = [\text{P}]_{\text{O}} - [\text{P}]_{\text{T}}$
(76)	$[\text{Al}^{3+}] \times [\text{PO}_4^{3-}] = 9.84 \times 10^{-21}$
(77)	$([\text{Al}]_{\text{O}} - [\text{Al}]_{\text{T}}) / ([\text{F}]_{\text{O}} - [\text{F}]_{\text{T}}) = 1/3$
(78)	$[\text{Al}^{3+}] \times [\text{F}^-]^3 = 4.53 \times 10^{-17}$
(79)	$([\text{P}]_{\text{O}} - [\text{P}]_{\text{T}}) - ([\text{Al}]_{\text{O}} - [\text{Al}]_{\text{T}}) / ([\text{Fe(II)}]_{\text{O}} - [\text{Fe(II)}]_{\text{T}}) = 2/3$
(80)	$(([\text{Al}]_{\text{O}} - [\text{Al}]_{\text{T}}) - ([\text{P}]_{\text{O}} - [\text{P}]_{\text{T}})) / ([\text{F}]_{\text{O}} - [\text{F}]_{\text{T}}) = 1/3$

Where [M] is the equilibrium concentration for each species; $[\text{P}]_{\text{T}}$, $[\text{Fe(II)}]_{\text{T}}$, $[\text{Li}]_{\text{T}}$, $[\text{S}]_{\text{T}}$, $[\text{Al}]_{\text{T}}$, and $[\text{F}]_{\text{T}}$ are designated as the total concentration of phosphate, Fe, Li, sulfate, Al, and F in equilibrium conditions; $[\text{P}]_{\text{O}}$, $[\text{Fe(II)}]_{\text{O}}$, $[\text{Li}]_{\text{O}}$, $[\text{S}]_{\text{O}}$, $[\text{Al}]_{\text{O}}$, and $[\text{F}]_{\text{O}}$ are defined as the initial total concentrations of phosphate, Fe, Li, sulfate, Al, and F before the precipitation of solid phases.

The possible stable regions of the $\text{Li}^+ - \text{Fe}^{2+} - \text{Al}^{3+} - \text{PO}_4^{3-} - \text{SO}_4^{2-} - \text{F}^- - \text{H}_2\text{O}$ system and their corresponding constraint equations are given in Table 6. By assigning values to $[\text{P}]_{\text{O}}$, $[\text{Fe(II)}]_{\text{O}}$, $[\text{Li}]_{\text{O}}$, $[\text{S}]_{\text{O}}$, $[\text{Al}]_{\text{O}}$, and $[\text{F}]_{\text{O}}$, the equations were solved using Microsoft Excel in accordance with the Newton-Raphson iteration method. In addition, the most thermodynamically stable region among all those possible corresponded to the lowest $[\text{Al}]_{\text{T}}$ and $[\text{F}]_{\text{T}}$ at a given pH value.

Table 6. Possible stable regions of $\text{Li}^+ - \text{Fe}^{2+} - \text{Al}^{3+} - \text{PO}_4^{3-} - \text{SO}_4^{2-} - \text{F}^- - \text{H}_2\text{O}$ system and their corresponding constraint equations.

No.	Stable Regions	Constraint Equations
1	Liquid phase	(3–16) + (29–43) + (66–72)
2	$\text{Fe}_3(\text{PO}_4)_2 \cdot 8\text{H}_2\text{O}_{(\text{s})}$	(3–16) + (29–43) + (66–74)
3	$\text{AlPO}_4_{(\text{s})}$	(3–16) + (29–43) + (66–72) + (75–76)
4	$\text{AlF}_3_{(\text{s})}$	(3–16) + (29–43) + (66–72) + (77–78)
5	$\text{Fe}_3(\text{PO}_4)_2 \cdot 8\text{H}_2\text{O}_{(\text{s})} + \text{AlPO}_4_{(\text{s})}$	(3–16) + (29–43) + (66–72) + (74) + (76) + (79)
6	$\text{Fe}_3(\text{PO}_4)_2 \cdot 8\text{H}_2\text{O}_{(\text{s})} + \text{AlF}_3_{(\text{s})}$	(3–16) + (29–43) + (66–74) + (77–78)
7	$\text{AlPO}_4_{(\text{s})} + \text{AlF}_3_{(\text{s})}$	(3–16) + (29–43) + (66–72) + (76) + (78) + (80)
8	$\text{Fe}_3(\text{PO}_4)_2 \cdot 8\text{H}_2\text{O}_{(\text{s})} + \text{AlPO}_4_{(\text{s})} + \text{AlF}_3_{(\text{s})}$	(3–16) + (29–43) + (66–72) + (74) + (76) + (78–79) + (80)

3.4. Thermodynamic Model of the $\text{Li}^+ - \text{Fe}^{3+} - \text{Al}^{3+} - \text{PO}_4^{3-} - \text{SO}_4^{2-} - \text{F}^- - \text{H}_2\text{O}$ System

The species in the solution of the $\text{Li}^+ - \text{Fe}^{3+} - \text{Al}^{3+} - \text{PO}_4^{3-} - \text{SO}_4^{2-} - \text{F}^- - \text{H}_2\text{O}$ system and their equilibrium equations are shown in Equations (3)–(8) and (17)–(43) in Table 1, respectively. In accordance with the simultaneous equilibrium principle, mass action law, and electroneutrality principle, Equations (81)–(87) were obtained.

$$[\text{P}]_{\text{T}} = [\text{PO}_4^{3-}] + [\text{HPO}_4^{2-}] + [\text{H}_2\text{PO}_4^-] + [\text{H}_3\text{PO}_4] + [\text{LiHPO}_4^-] + [\text{FeHPO}_4^+] + [\text{FeH}_2\text{PO}_4^{2+}] \quad (81)$$

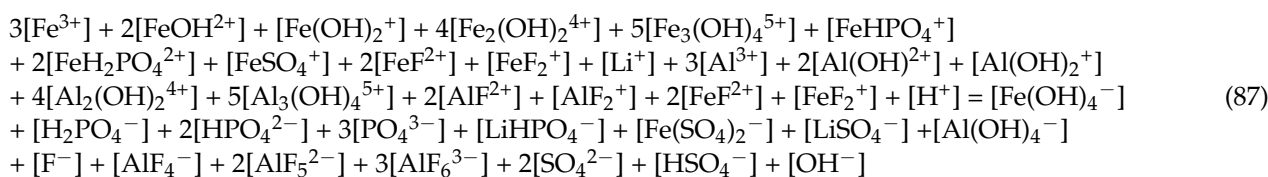
$$[\text{Fe(III)}]_{\text{T}} = [\text{Fe}^{3+}] + [\text{FeOH}^{2+}] + [\text{Fe(OH)}_2^+] + [\text{Fe(OH)}_4^-] + 2[\text{Fe}_2(\text{OH})_2^{4+}] + 3[\text{Fe}_3(\text{OH})_4^{5+}] + [\text{FeHPO}_4^+] + [\text{FeH}_2\text{PO}_4^{2+}] + [\text{FeF}^{2+}] + [\text{FeF}_2^+] + [\text{FeF}_3(\text{aq})] + [\text{FeSO}_4^+] + [\text{Fe(SO}_4)_2^-] \quad (82)$$

$$[\text{Li}]_{\text{T}} = [\text{Li}^+] + [\text{Li(OH)}_{(\text{aq})}] + [\text{LiSO}_4^-] + [\text{LiHPO}_4^-] \quad (83)$$

$$[\text{S}]_{\text{T}} = [\text{SO}_4^{2-}] + [\text{H}_2\text{SO}_4] + [\text{HSO}_4^-] + [\text{FeSO}_4^+] + 2[\text{Fe(SO}_4)_2^-] + [\text{LiSO}_4^-] \quad (84)$$

$$[\text{Al}]_{\text{T}} = [\text{Al}^{3+}] + [\text{AlF}^{2+}] + [\text{AlF}_2^+] + [\text{AlF}_3(\text{aq})] + [\text{AlF}_4^-] + [\text{AlF}_5^{2-}] + [\text{AlF}_6^{3-}] + [\text{Al(OH)}_2^{2+}] + [\text{Al(OH)}_2^+] + [\text{Al(OH)}_3(\text{aq})] + [\text{Al(OH)}_4^-] + 2[\text{Al}_2(\text{OH})_2^{4+}] + 3[\text{Al}_3(\text{OH})_4^{5+}] \quad (85)$$

$$[\text{F}]_{\text{T}} = [\text{F}^-] + [\text{AlF}^{2+}] + 2[\text{AlF}_2^+] + 3[\text{AlF}_3(\text{aq})] + 4[\text{AlF}_4^-] + 5[\text{AlF}_5^{2-}] + 6[\text{AlF}_6^{3-}] + [\text{FeF}^+] \quad (86)$$



When a solid phase is formed in the system, each component in the solid phase stable region must meet Equations (3)–(8), (17)–(43), and (81)–(87), as well as their corresponding constraint equations. The constraint equations for different solid phase stable regions are given in Table 7.

Table 7. Constraint equations for different solid phase stable region.

Eq no	Equation
(88)	$[\text{Fe}(\text{III})]_{\text{O}} - [\text{Fe}(\text{III})]_{\text{T}} = [\text{P}]_{\text{O}} - [\text{P}]_{\text{T}}$
(89)	$[\text{Fe}^{3+}] \times [\text{PO}_4^{3-}] = 1.3 \times 10^{-22}$
(90)	$[\text{Al}]_{\text{O}} - [\text{Al}]_{\text{T}} = [\text{P}]_{\text{O}} - [\text{P}]_{\text{T}}$
(91)	$[\text{Al}^{3+}] \times [\text{PO}_4^{3-}] = 9.84 \times 10^{-21}$
(92)	$([\text{Fe}(\text{III})]_{\text{O}} - [\text{Fe}(\text{III})]_{\text{T}}) / ([\text{F}]_{\text{O}} - [\text{F}]_{\text{T}}) = 1/3$
(93)	$[\text{Fe}^{3+}] \times [\text{F}^-]^3 = 1.089 \times 10^{-36}$
(94)	$[\text{Fe}^{3+}] \times [\text{OH}^-]^3 = 10^{-38.8}$
(95)	$([\text{P}]_{\text{O}} - [\text{P}]_{\text{T}}) / ([\text{Fe}(\text{III})]_{\text{O}} - [\text{Fe}(\text{III})]_{\text{T}}) + ([\text{Al}]_{\text{O}} - [\text{Al}]_{\text{T}}) = 1$
(96)	$([\text{Fe}(\text{III})]_{\text{O}} - [\text{Fe}(\text{III})]_{\text{T}}) / ([\text{P}]_{\text{O}} - [\text{P}]_{\text{T}}) + ([\text{F}]_{\text{O}} - [\text{F}]_{\text{T}}) = 1$

Where [M] is the equilibrium concentration for each species; $[\text{P}]_{\text{T}}$, $[\text{Fe}(\text{III})]_{\text{T}}$, $[\text{Li}]_{\text{T}}$, $[\text{S}]_{\text{T}}$, $[\text{Al}]_{\text{T}}$, and $[\text{F}]_{\text{T}}$ are designated as the total concentration of phosphate, Fe, Li, sulfate, Al, and F in equilibrium conditions; $[\text{P}]_{\text{O}}$, $[\text{Fe}(\text{III})]_{\text{O}}$, $[\text{Li}]_{\text{O}}$, $[\text{S}]_{\text{O}}$, $[\text{Al}]_{\text{O}}$, and $[\text{F}]_{\text{O}}$ are defined as the initial total concentrations of phosphate, Fe, Li, sulfate, Al, and F before the precipitation of solid phases.

The possible stable regions of the $\text{Li}^+ - \text{Fe}^{3+} - \text{Al}^{3+} - \text{PO}_4^{3-} - \text{SO}_4^{2-} - \text{F}^- - \text{H}_2\text{O}$ system and their corresponding constraint equations are presented in Table 8. The equations were solved using Microsoft Excel by assigning values to $[\text{P}]_{\text{O}}$, $[\text{Fe}(\text{III})]_{\text{O}}$, $[\text{Li}]_{\text{O}}$, $[\text{S}]_{\text{O}}$, $[\text{Al}]_{\text{O}}$, and $[\text{F}]_{\text{O}}$ on the basis of the Newton-Raphson iteration method. Moreover, the most thermodynamically stable region among all possible ones corresponded to the lowest $[\text{Al}]_{\text{T}}$ and $[\text{F}]_{\text{T}}$ at a given pH value.

Table 8. Possible stable regions of $\text{Li}^+ - \text{Fe}^{3+} - \text{Al}^{3+} - \text{PO}_4^{3-} - \text{SO}_4^{2-} - \text{F}^- - \text{H}_2\text{O}$ system and their corresponding constraint equations.

No.	Stable Regions	Constraint Equations
1	Liquid phase	(3–8) + (17–43) + (81–87)
2	$\text{FePO}_4(\text{s})$	(3–8) + (17–43) + (81–87)
3	$\text{AlPO}_4(\text{s})$	(3–8) + (17–43) + (81–87) + (90–91)
4	$\text{FeF}_3(\text{s})$	(3–8) + (17–43) + (81–87) + (92–93)
5	$\text{Fe}(\text{OH})_3(\text{s})$	(3–8) + (17–43) + (81–87) + (94)
6	$\text{FePO}_4(\text{s}) + \text{AlPO}_4(\text{s})$	(3–8) + (17–43) + (81–87) + (89) + (91) + (95)
7	$\text{FePO}_4(\text{s}) + \text{FeF}_3(\text{s})$	(3–8) + (17–43) + (81–87) + (89) + (93) + (96)
8	$\text{FePO}_4(\text{s}) + \text{Fe}(\text{OH})_3(\text{s})$	(3–8) + (17–43) + (81–87) + (89) + (94)
9	$\text{AlPO}_4(\text{s}) + \text{FeF}_3(\text{s})$	(3–8) + (17–43) + (81–87) + (90–93)
10	$\text{AlPO}_4(\text{s}) + \text{Fe}(\text{OH})_3(\text{s})$	(3–8) + (17–43) + (81–87) + (90–91) + (94)
11	$\text{FeF}_3(\text{s}) + \text{Fe}(\text{OH})_3(\text{s})$	(3–8) + (17–43) + (81–87) + (93–94)
12	$\text{FePO}_4(\text{s}) + \text{AlPO}_4(\text{s}) + \text{FeF}_3(\text{s})$	(3–8) + (17–43) + (81–87) + (89) + (91) + (93) + (95) + (96)
13	$\text{FePO}_4(\text{s}) + \text{AlPO}_4(\text{s}) + \text{Fe}(\text{OH})_3(\text{s})$	(3–8) + (17–43) + (81–87) + (89) + (91) + (94)
14	$\text{AlPO}_4(\text{s}) + \text{FeF}_3(\text{s}) + \text{Fe}(\text{OH})_3(\text{s})$	(3–8) + (17–43) + (81–87) + (90–91) + (93–94)
15	$\text{FePO}_4(\text{s}) + \text{FeF}_3(\text{s}) + \text{Fe}(\text{OH})_3(\text{s})$	(3–8) + (17–43) + (81–87) + (89) + (93–94)
16	$\text{FePO}_4(\text{s}) + \text{AlPO}_4(\text{s}) + \text{FeF}_3(\text{s}) + \text{Fe}(\text{OH})_3(\text{s})$	(3–8) + (17–43) + (81–87) + (89) + (91) + (93–94)

4. Results and Discussion

4.1. $\text{Li}^+ - \text{Fe}^{2+} - \text{Al}^{3+} - \text{PO}_4^{3-} - \text{SO}_4^{2-} - \text{F}^- - \text{H}_2\text{O}$ System

Figure 2 shows the element equilibrium total concentration and the solid phases distribution of the $\text{Li}^+ - \text{Fe}^{2+} - \text{Al}^{3+} - \text{PO}_4^{3-} - \text{SO}_4^{2-} - \text{F}^- - \text{H}_2\text{O}$ system at the initial concentration of 1 M $[\text{P}]_0$, 1 M $[\text{Fe}]_0$, 0.8 M $[\text{Li}]_0$, 1.5 M $[\text{S}]_0$, 0.02 M $[\text{Al}]_0$, and 0.02 M $[\text{F}]_0$. At $\text{pH} < 1.5$, the total concentration of each element in the solution remained constant and no precipitation was generated. At $1.5 \leq \text{pH} \leq 2.6$, the total concentration of aluminum ions and phosphate ions decreased because the reaction of aluminum ions and phosphate ions formed AlPO_4 precipitate (Figure 2b). AlPO_4 was the main precipitate at $\text{pH} = 1.5 - 2.6$. At $\text{pH} \geq 2.6$, the total concentration of iron ions decreased and that of phosphate ions decreased more sharply because the reaction of ferrous ions and phosphate ions formed $\text{Fe}_3(\text{PO}_4)_2 \cdot 8\text{H}_2\text{O}$ precipitate. Accordingly, the precipitates generated in the solution included AlPO_4 and $\text{Fe}_3(\text{PO}_4)_2 \cdot 8\text{H}_2\text{O}$ when the pH value was above 2.5, and the molar proportion of $\text{Fe}_3(\text{PO}_4)_2 \cdot 8\text{H}_2\text{O}$ increased as the final pH value increased. At $\text{pH} \geq 3.0$, the molar proportion of $\text{Fe}_3(\text{PO}_4)_2 \cdot 8\text{H}_2\text{O}$ and AlPO_4 remained stable, and $\text{Fe}_3(\text{PO}_4)_2 \cdot 8\text{H}_2\text{O}$ was the main precipitate, AlPO_4 was the minor precipitate.

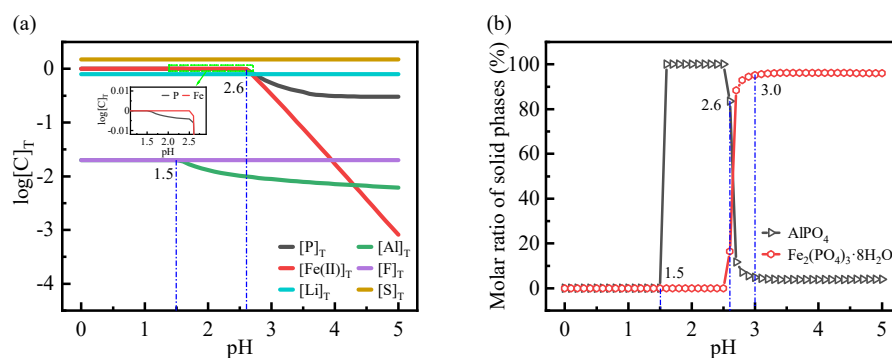


Figure 2. (a) Elements equilibrium total concentration and (b) solid phases distribution of the $\text{Li}^+ - \text{Fe}^{2+} - \text{Al}^{3+} - \text{PO}_4^{3-} - \text{SO}_4^{2-} - \text{F}^- - \text{H}_2\text{O}$ system (298 K, $[\text{P}]_0 = [\text{Fe(II)}]_0 = 1$ M, $[\text{Li}]_0 = 0.8$ M, $[\text{S}]_0 = 1.5$ M, $[\text{Al}]_0 = [\text{F}]_0 = 0.02$ M).

4.2. $\text{Li}^+ - \text{Fe}^{3+} - \text{Al}^{3+} - \text{PO}_4^{3-} - \text{SO}_4^{2-} - \text{F}^- - \text{H}_2\text{O}$ System

Figure 3 presents the element equilibrium total concentration and the solid phases distribution of the $\text{Li}^+ - \text{Fe}^{3+} - \text{Al}^{3+} - \text{PO}_4^{3-} - \text{SO}_4^{2-} - \text{F}^- - \text{H}_2\text{O}$ system at the initial concentration of 1 M $[\text{P}]_0$, 1 M $[\text{Fe}]_0$, 0.8 M $[\text{Li}]_0$, 1.5 M $[\text{S}]_0$, 0.02 M $[\text{Al}]_0$, and 0.02 M $[\text{F}]_0$. At $\text{pH} = 0$, the total concentration of iron and fluoride ions was lower than the initial value, indicating that the formation of FeF_3 precipitate in the $\text{Li}^+ - \text{Fe}^{3+} - \text{Al}^{3+} - \text{PO}_4^{3-} - \text{SO}_4^{2-} - \text{F}^- - \text{H}_2\text{O}$ system decreased the total concentration of ferric ions and fluorine ions (Figure 3b). FeF_3 was the only precipitate at $\text{pH} \leq 0.8$. At $\text{pH} = 0 - 1.4$, the total concentration of fluoride ion continuously increased, suggesting that the increase in pH value within the range was not conducive to the formation of FeF_3 . At $\text{pH} \geq 0.8$, the total concentration of phosphate ions and iron ions substantially decreased because of the formation of FePO_4 . At $\text{pH} \geq 1.4$, the total concentration of aluminum ions began to decrease owing to the formation of AlPO_4 , whereas the concentration of fluoride ions also began to decrease because of the formation of FeF_3 . At $\text{pH} = 1.0 - 3.9$, FePO_4 was the main precipitate, FeF_3 and AlPO_4 were the minor precipitate. At $\text{pH} \geq 3.9$, the total concentration of phosphate ions started to increase, because of the disappearance of FePO_4 and the mass formation of $\text{Fe}(\text{OH})_3$ with the increase in concentration of hydroxide ions. At $\text{pH} \geq 4.0$, the molar proportion of FeF_3 , AlPO_4 , and $\text{Fe}(\text{OH})_3$ precipitate remained stable, and $\text{Fe}(\text{OH})_3$ was the main precipitate, FeF_3 and AlPO_4 was the minor precipitate.

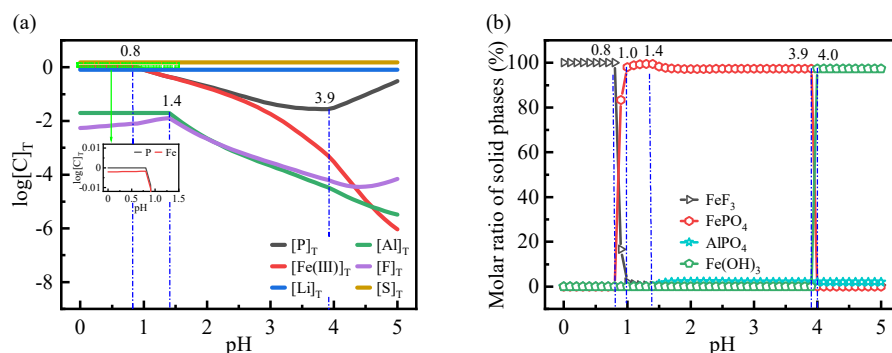


Figure 3. (a) Elements equilibrium total concentration and (b) solid phases distribution of the $\text{Li}^+ - \text{Fe}^{3+} - \text{Al}^{3+} - \text{PO}_4^{3-} - \text{SO}_4^{2-} - \text{F}^- - \text{H}_2\text{O}$ system (298 K, $[\text{P}]_{\text{O}} = [\text{Fe(III)}]_{\text{O}} = 1 \text{ M}$, $[\text{Li}]_{\text{O}} = 0.8 \text{ M}$, $[\text{S}]_{\text{O}} = 1.5 \text{ M}$, $[\text{Al}]_{\text{O}} = [\text{F}]_{\text{O}} = 0.02 \text{ M}$).

4.3. Precipitation Experiments

Based on the results of above thermodynamic modeling calculation, the sulfuric acid leachate of spent LiFePO_4 battery powder was employed to conduct bench-scale experiments to validate the feasibility of the separation and purification technology under the conditions of the reaction temperature of $25 \text{ }^\circ\text{C}$, reaction time of 5 min, and agitation rate of 400 rpm.

Figure 4 shows the effects of $\text{Na}_3\text{PO}_4 \cdot 12\text{H}_2\text{O}$ dosage on the final pH value and precipitation behavior of each element in the solution. Figure 4a depicts the relationship between $\text{Na}_3\text{PO}_4 \cdot 12\text{H}_2\text{O}$ dosage and the final pH value of the 250 mL solution. As indicated in Figure 4b,c, the final pH value of the solution had a considerable effect on the removal of aluminum and fluorine impurities by chemical precipitation. When the amount of $\text{Na}_3\text{PO}_4 \cdot 12\text{H}_2\text{O}$ added was increased from 21.4 g to 25.3 g, the final pH value increased from 3.05 to 3.77. Correspondingly, the concentration of residual aluminum ions in the solution decreased from 890.5 mg/L to 27.55 mg/L. Moreover, the removal rate of aluminum ions increased from 55.48% to 98.62%, the concentration of residual fluoride ions decreased from 490.5 mg/L to 46.0 mg/L, and the removal rate of aluminum ions increased from 51.1% to 95.41%. By comparison, when the final pH value increased to 3.90, the concentration of residual aluminum and fluoride ions only slightly decreased from 27.55 mg/L to 15.95 mg/L and from 46.0 mg/L to 39.78 mg/L, respectively. The effects of the final pH value on PO_4^{3-} , Fe^{2+} , and Li^+ in the solution are illustrated in Figure 4d–f, respectively. As presented in Figure 4d, e, the loss rate of PO_4^{3-} and Fe^{2+} increased, when the final pH value increased from 3.05 to 3.77. Combined with the results of thermodynamic calculation, the increase in the loss rate of PO_4^{3-} and Fe^{2+} should be resulted by the formation of FeF_3 , AlPO_4 , $\text{Fe}_3(\text{PO}_4)_2 \cdot 8\text{H}_2\text{O}$, FePO_4 , and $\text{Fe}(\text{OH})_3$. When the final pH value increased from 3.05 to 3.90, the loss rate of Li^+ slightly increased from 0.21% to 2.28% (Figure 4f). The high final pH value probably resulted in an increase in the amount of precipitation that contained lithium ions. In conclusion, the final pH value at about 3.77 could deeply purify the aluminum ions and fluoride ions, as well as reduce the loss rate of phosphate ions and iron ions as much as possible.

The XRD patterns and FT-IR spectra of precipitation obtained at different final pH values are plotted in Figure 5. As shown in Figure 5a, no obvious characteristic diffraction peak appeared on the XRD pattern, demonstrating that the precipitation had an amorphous structure. Figure 5b shows the FTIR spectra of precipitation. The wide absorption peak at 3424 cm^{-1} and the small absorption peak at 1630 cm^{-1} corresponded to the O–H bond stretching and bending vibrations in the precipitation, respectively [12]. The strong absorption peak at 1090 cm^{-1} was attributed to the P–O stretching vibrations in PO_4^{3-} [37]. The small absorption peak at 617 cm^{-1} represented the Al–O stretching vibrations in tetrahedral AlO_4^{5-} [38], and the absorption peak at 530 cm^{-1} corresponded to the Fe–O stretching vibrations [38]. According to the FTIR spectra of precipitation and the results

of thermodynamic simulation calculation, the main compositions of precipitation were AlPO_4 , $\text{Fe}_3(\text{PO}_4)_2 \cdot 8\text{H}_2\text{O}$, FePO_4 , and $\text{Fe}(\text{OH})_3$.

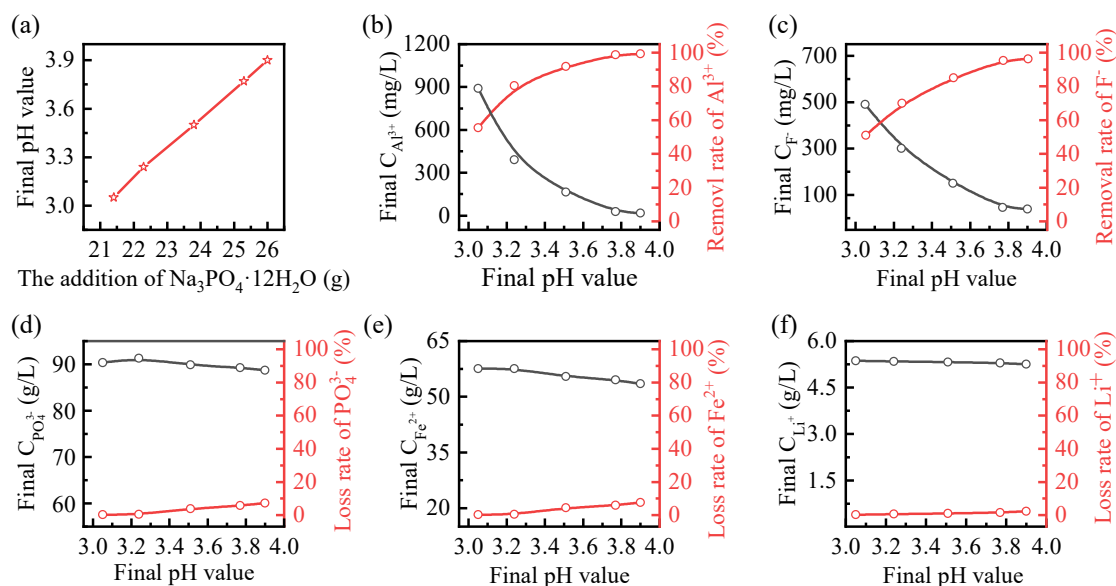


Figure 4. Effects of (a) $\text{Na}_3\text{PO}_4 \cdot 12\text{H}_2\text{O}$ dosage on the final pH value and precipitation behavior of (b) Al^{3+} , (c) F^- , (d) PO_4^{3-} and (e) Fe^{2+} and (f) Li^+ .

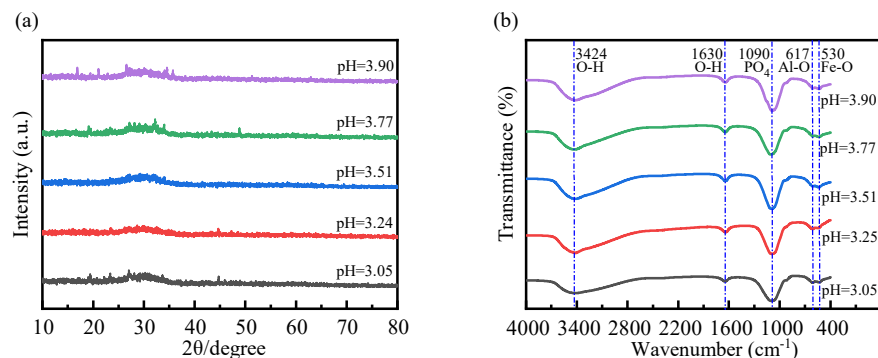


Figure 5. (a) X-ray diffraction (XRD) patterns and (b) Fourier transform infrared (FTIR) spectra of precipitate at different final pH value. (agitation rate = 400 rpm, reaction time = 5 min, and reaction temperature = 25 °C).

The SEM–EDS spectra of precipitation under the optimal conditions are presented in Figure 6. Figure 6a shows that the precipitation was inside small irregular particles. Figure 6b is a partially enlarged map of precipitation, and its EDS mapping indicated that the precipitation contained various elements, such as P, Fe, O, Al, and F.

The phase composition and surface chemical states of precipitation was further characterized via XPS analysis (Figure 7). The P 2p spectrum in Figure 7a shows that the peaks corresponding to the binding energies of P 2p_{3/2} and P 2p_{1/2} were located at 133.6 and 134.4 eV, respectively, which were caused by spin-orbit coupling. This result was consistent with the reported binding energies of P–O in PO_4^{3-} [39]. The Fe 2P spectrum in Figure 7b shows that the spin-orbit doublets of Fe 2p_{3/2} and Fe 2p_{1/2} were situated at approximately 712.0 and 725.0 eV, respectively. Each of them consisted of two main peaks (709.4 and 711.3 eV for Fe 2p_{3/2}, 722.5 and 724.4 eV for Fe 2p_{1/2}) and two satellites (713.9 and 717.3 eV for Fe 2p_{3/2}, 727.0 and 730.4 eV for Fe 2p_{1/2}) [40]. The results indicated that the iron element in the precipitation existed in the form of Fe^{2+} and Fe^{3+} , and the $\text{Fe}^{3+}/\text{Fe}^{2+}$ molar ratio was 1.35. Owing to the overlapping photoelectron spectra of Li 1s and Fe 3p,

Gaussian peak fitting was performed for Li 1s (Figure 7c). The characteristic peak of Li 1s located at 56.6 eV was attributed to Li^+ [40]. The O 1s spectrum was fitted with two peaks (Figure 7d). The strong peak at 531.3 eV was related to the P–O of phosphate groups, whereas the weak peak at 532.8 eV was associated with O–H. The characteristic peaks of Al 2p that appeared at 74.7 and 75.1 eV were related to Al–O from AlPO_4 (Figure 7e), indicating that the aluminum element in the precipitation existed in the form of AlPO_4 . Figure 7f shows the spectrum of F 1s. The characteristic peak of F 1s centered at 68.5 eV as ascribed to Fe–F. Therefore, the fluorine element in the precipitation existed as FeF_3 .

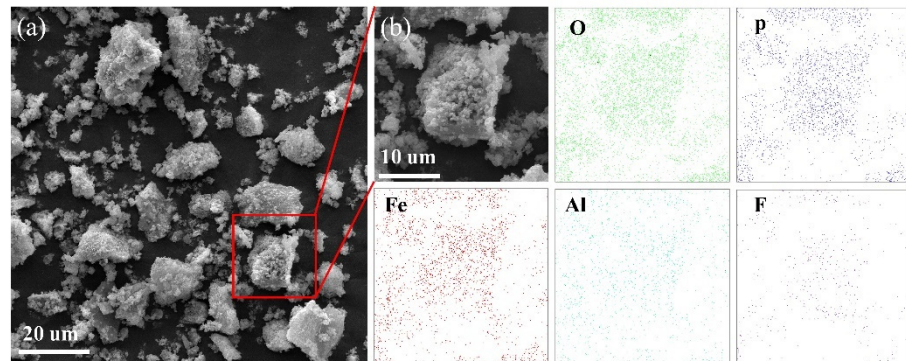


Figure 6. Scanning electron microscopy-energy-dispersive spectroscopy (SEM-EDS) spectra of precipitate under optimal conditions. (agitation rate = 400 rpm, reaction time = 5 min, reaction temperature = 25 °C, and final pH value 3.77). (a) SEM image of the precipitate; (b) Microstructure of the precipitate.

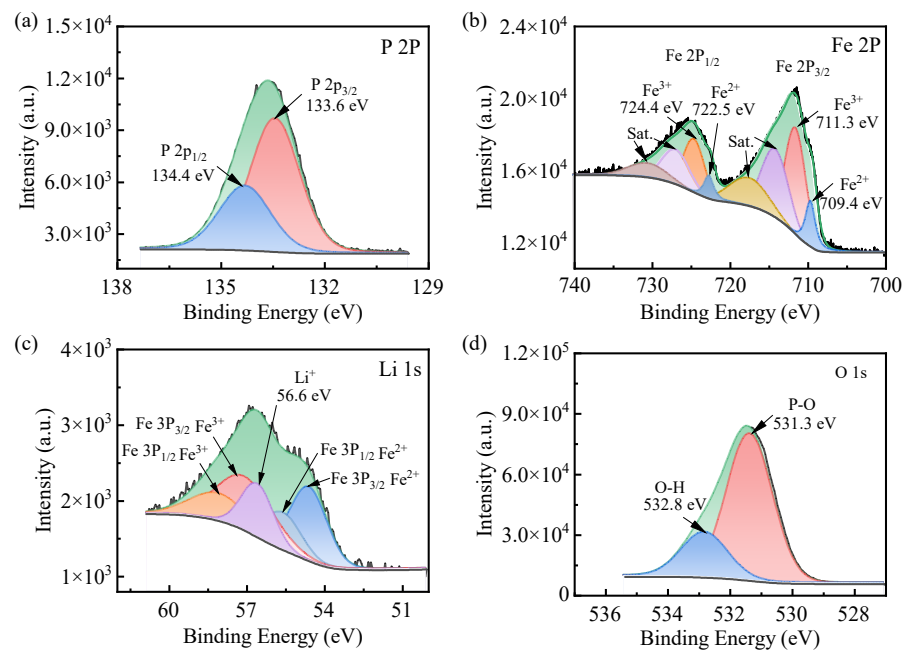


Figure 7. Cont.

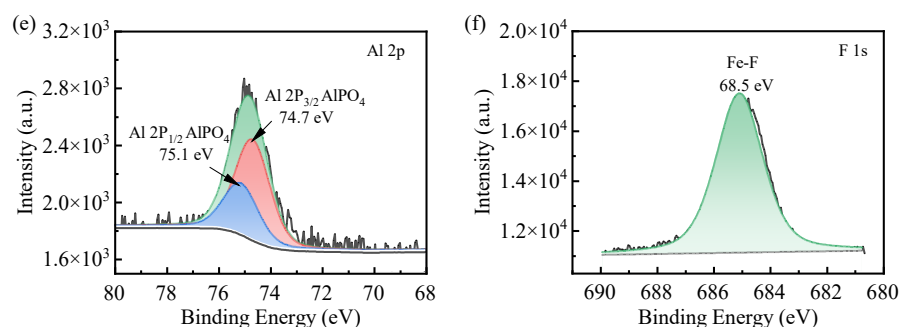


Figure 7. X-ray photoelectron spectroscopy (XPS) spectra of precipitate under optimal conditions. (agitation rate = 400 rpm, reaction time = 5 min, reaction temperature = 25 °C, and final pH value 3.77). (a) P 2p; (b) Fe 2p; (c) Li 1s; (d) O 1s; (e) Al 2p; (f) F 1s.

5. Conclusions

The evolution law of the total equilibrium concentration of Al, Fe, P, and F, and the phase composition of precipitates at different final pH values are explained using the thermodynamic mathematical model. By adjusting the final pH value of the $\text{Li}^+ - \text{Fe}^{2+} / \text{Fe}^{3+} - \text{PO}_4^{3-} - \text{SO}_4^{2-} - \text{H}_2\text{O}$ system, Al and F elements were precipitated in solid phases of AlPO_4 , and FeF_3 , whereas P and Fe elements were co-precipitated as $\text{Fe}_3(\text{PO}_4)_2 \cdot 8\text{H}_2\text{O}$, FePO_4 , and $\text{Fe}(\text{OH})_3$, respectively. Among them, $\text{Fe}_3(\text{PO}_4)_2 \cdot 8\text{H}_2\text{O}$ is the main precipitate, and the precipitate also contains a small amount of FePO_4 , $\text{Fe}(\text{OH})_3$, AlPO_4 , and FeF_3 . Therefore, selective precipitation of Al^{3+} and F^- can be precisely controlled by pH of the leaching solution, at the same time, the loss rate of P and Fe can be reduced. The removal mechanism of Al and F was further revealed by characterizing the precipitation via XRD, FTIR, SEM-EDS, and XPS. Results indicated that the precipitation mainly existed in the form of AlPO_4 , $\text{Fe}_3(\text{PO}_4)_2 \cdot 8\text{H}_2\text{O}$, FePO_4 , $\text{Fe}(\text{OH})_3$, and FeF_3 , consistent with the results of thermodynamic analysis.

Author Contributions: Conceptualization, S.Y. and Y.L.; methodology, Z.L. and Y.C.; software, Y.J.; validation, Y.C., S.Y. and Y.L.; formal analysis, P.S.; investigation, D.C.; resources, Y.C.; data curation, G.F.; writing—original draft preparation, Y.J.; writing—review and editing, Y.J., C.M. and J.D.; visualization, Y.C.; supervision, Z.L., S.Y. and Y.L.; project administration, Y.C.; funding acquisition, S.Y. and Y.C. All authors have read and agreed to the published version of the manuscript.

Funding: This work was funded by the Hunan Provincial Key Research and Development Projects (Social Development) (Grant No. 2019SK2061) as well as the Research Fund Program of State Key Laboratory of Separation and Comprehensive Utilization of Rare Metals (No. GK-201806). We are sincerely grateful for their help in this research project.

Data Availability Statement: Data is contained within the article.

Conflicts of Interest: The authors declare no conflict of interest.

References

1. Arens, M.; Åhman, M.; Vogl, V. Which countries are prepared to green their coal-based steel industry with electricity?—Reviewing climate and energy policy as well as the implementation of renewable electricity. *Renew. Sustain. Energy Rev.* **2021**, *143*, 110938. [[CrossRef](#)]
2. Mallapaty, S. How China could be carbon neutral by mid-century. *Nature* **2020**, *586*, 482–483. [[CrossRef](#)]
3. Bu, C.; Cui, X.; Li, R.; Li, J.; Zhang, Y.; Wang, C.; Cai, W. Achieving net-zero emissions in China's passenger transport sector through regionally tailored mitigation strategies. *Appl. Energy* **2021**, *284*, 116265. [[CrossRef](#)]
4. Wu, W.; Zhai, C.; Sui, Y.; Zhang, H. A novel distributed energy system using high-temperature proton exchange membrane fuel cell integrated with hybrid-energy heat pump. *Energy Convers. Manag.* **2021**, *235*, 113990. [[CrossRef](#)]
5. Sommerville, R.; Zhu, P.; Rajaeifar, M.A.; Heidrich, O.; Goodship, V.; Kendrick, E. A qualitative assessment of lithium ion battery recycling processes. *Resour. Conserv. Recycl.* **2021**, *165*, 105219. [[CrossRef](#)]
6. Yang, D.; Du, T.; Gong, H.; Luo, W. The Current Process for the Recycling of Spent Lithium Ion Batteries. *Front. Chem.* **2020**, *8*, 578044.

7. China EV 100, Power Battery Life Cycle Asset Operation Management Research. Available online: http://www.ev100plus.com/content/details1017_4298.html (accessed on 11 May 2021).
8. Gu, S.; Zhang, L.; Fu, B.; Wang, X.; Ahn, J.W. Feasible route for the recovery of strategic metals from mixed lithium-ion batteries cathode materials by precipitation and carbonation. *Chem. Eng. J.* **2020**, *420*, 127561. [[CrossRef](#)]
9. Liu, F.; Peng, C.; Ma, Q.; Wang, J.; Zhou, S.; Chen, Z.; Wilson, B.P.; Lundström, M. Selective lithium recovery and integrated preparation of high-purity lithium hydroxide products from spent lithium-ion batteries. *Sep. Purif. Technol.* **2021**, *259*, 118181. [[CrossRef](#)]
10. Zhao, Y.; Yuan, X.; Jiang, L.; Wen, J.; Wang, H.; Guan, R.; Zhang, J.; Zeng, G. Regeneration and reutilization of cathode materials from spent lithium-ion batteries. *Chem. Eng. J.* **2020**, *383*, 123089. [[CrossRef](#)]
11. Wang, S.; Zhang, Z.; Lu, Z.; Xu, Z. A novel method for screening deep eutectic solvent to recycle the cathode of Li-ion batteries. *Green Chem.* **2020**, *22*, 4473–4482. [[CrossRef](#)]
12. Jie, Y.; Yang, S.; Li, Y.; Hu, F.; Zhao, D.; Chang, D.; Lai, Y.; Chen, Y. Waste Organic Compounds Thermal Treatment and Valuable Cathode Materials Recovery from Spent LiFePO₄ Batteries by Vacuum Pyrolysis. *ACS Sustain. Chem. Eng.* **2020**, *8*, 19084–19095. [[CrossRef](#)]
13. Huang, B.; Pan, Z.; Su, X.; An, L. Recycling of lithium-ion batteries: Recent advances and perspectives. *J. Power Sources* **2018**, *399*, 274–286. [[CrossRef](#)]
14. Yang, Y.; Meng, X.; Cao, H.; Lin, X.; Liu, C.; Sun, Y.; Zhang, Y.; Sun, Z. Selective recovery of lithium from spent lithium iron phosphate batteries: A sustainable process. *Green Chem.* **2018**, *20*, 3121–3133. [[CrossRef](#)]
15. Li, H.; Xing, S.; Liu, Y.; Li, F.; Guo, H.; Kuang, G. Recovery of Lithium, Iron, and Phosphorus from Spent LiFePO₄ Batteries Using Stoichiometric Sulfuric Acid Leaching System. *ACS Sustain. Chem. Eng.* **2017**, *5*, 8017–8024. [[CrossRef](#)]
16. Zheng, R.; Zhao, L.; Wang, W.; Liu, Y.; Ma, Q.; Mu, D.; Li, R.; Dai, C. Optimized Li and Fe recovery from spent lithium-ion batteries via a solution-precipitation method. *RSC Adv.* **2016**, *6*, 43613–43625. [[CrossRef](#)]
17. Cai, G.; Fung, K.Y.; Ng, K.M. Process Development for the Recycle of Spent Lithium Ion Batteries by Chemical Precipitation. *Ind. Eng. Chem. Res.* **2014**, *53*, 18245–18259. [[CrossRef](#)]
18. Huang, Y.; Han, G.; Liu, J.; Chai, W.; Wang, W.; Yang, S.; Su, S. A stepwise recovery of metals from hybrid cathodes of spent Li-ion batteries with leaching-flotation-precipitation process. *J. Power Sources* **2016**, *325*, 555–564. [[CrossRef](#)]
19. Shin, E.J.; Kim, S.; Noh, J.K.; Byun, D.; Chung, K.Y.; Kim, H.S.; Cho, B.W. A green recycling process designed for LiFePO₄ cathode materials for Li-ion batteries. *J. Mater. Chem. A* **2015**, *3*, 11493–11502. [[CrossRef](#)]
20. Chen, X.; Li, J.; Kang, D.; Zhou, T.; Ma, H. A novel closed-loop process for the simultaneous recovery of valuable metals and iron from a mixed type of spent lithium-ion batteries. *Green Chem.* **2019**, *21*, 6342–6352. [[CrossRef](#)]
21. Chen, X.; Cao, L.; Kang, D.; Li, J.; Zhou, T.; Ma, H. Recovery of valuable metals from mixed types of spent lithium ion batteries. Part II: Selective extraction of lithium. *Waste Manag.* **2018**, *80*, 198–210. [[CrossRef](#)]
22. Yang, Y.; Zheng, X.; Cao, H.; Zhao, C.; Lin, X.; Ning, P.; Zhang, Y.; Jin, W.; Sun, Z. A Closed-Loop Process for Selective Metal Recovery from Spent Lithium Iron Phosphate Batteries through Mechanochemical Activation. *ACS Sustain. Chem. Eng.* **2017**, *5*, 9972–9980. [[CrossRef](#)]
23. Bian, D.; Sun, Y.; Li, S.; Tian, Y.; Yang, Z.; Fan, X.; Zhang, W. A novel process to recycle spent LiFePO₄ for synthesizing LiFePO₄/C hierarchical microflowers. *Electrochim. Acta* **2016**, *190*, 134–140. [[CrossRef](#)]
24. Li, L.; Lu, J.; Zhai, L.; Zhang, X.; Curtiss, L.; Jin, Y.; Wu, F.; Chen, R.; Amine, K. A facile recovery process for cathodes from spent lithium iron phosphate batteries by using oxalic acid. *CSEE J. Power Energy* **2018**, *4*, 219–225. [[CrossRef](#)]
25. Fan, E.; Li, L.; Zhang, X.; Bian, Y.; Xue, Q.; Wu, J.; Wu, F.; Chen, R. Selective Recovery of Li and Fe from Spent Lithium-Ion Batteries by an Environmentally Friendly Mechanochemical Approach. *ACS Sustain. Chem. Eng.* **2018**, *6*, 11029–11035. [[CrossRef](#)]
26. Yadava, P.; Jie, C.J.; Tanb, S.; Srinivasan, M. Recycling of cathode from spent lithium iron phosphate batteries. *J. Hazard. Mater.* **2020**, *399*, 123068. [[CrossRef](#)]
27. Yao, Y.; Zhu, M.; Zhao, Z.; Tong, B.; Fan, Y.; Hua, Z. Hydrometallurgical Processes for Recycling Spent Lithium-Ion Batteries: A Critical Review. *ACS Sustain. Chem. Eng.* **2018**, *6*, 13611–13627. [[CrossRef](#)]
28. Lv, W.; Wang, Z.; Cao, H.; Sun, Y.; Zhang, Y.; Sun, Z. A Critical Review and Analysis on the Recycling of Spent Lithium-Ion Batteries. *ACS Sustain. Chem. Eng.* **2018**, *6*, 1504–1521. [[CrossRef](#)]
29. Pagnanelli, F.; Moscardini, E.; Altimari, P.; Abo Atia, T.; Toro, L. Cobalt products from real waste fractions of end of life lithium ion batteries. *Waste Manag.* **2016**, *51*, 214–221. [[CrossRef](#)]
30. Joo, S.H.; Shin, D.; Oh, C.H.; Wang, J.; Senanayake, G.; Shin, S.M. Selective extraction and separation of nickel from cobalt, manganese and lithium in pre-treated leach liquors of ternary cathode material of spent lithium-ion batteries using synergism caused by Versatic 10 acid and LIX 84-I. *Hydrometallurgy* **2016**, *159*, 65–74. [[CrossRef](#)]
31. Kang, J.; Senanayake, G.; Sohn, J.; Shin, S.M. Recovery of cobalt sulfate from spent lithium ion batteries by reductive leaching and solvent extraction with Cyanex 272. *Hydrometallurgy* **2010**, *100*, 168–171. [[CrossRef](#)]
32. Weng, Y.; Xu, S.; Huang, G.; Jiang, C. Synthesis and performance of Li[(Ni_{1/3}Co_{1/3}Mn_{1/3})_{1-x}Mg_x]O₂ prepared from spent lithium ion batteries. *J. Hazard. Mater.* **2013**, *246–247*, 163–172. [[CrossRef](#)]
33. Hsu, P.H. Precipitation of phosphate from solution using aluminum salt. *Water Res.* **1975**, *9*, 1155–1161.
34. Speight, J.G. *Lange's Handbook of Chemistry*, 6th ed.; McGraw-Hill: New York, NY, USA, 2005.

35. Roine, A. HSC Chemistry 9.2.6. Outotec Research Oy, Pori, Finland. 2019. Available online: <http://www.chemistry-software.com/> (accessed on 11 May 2021).
36. Bale, C.W.; Chartrand, P.; Degterov, S.A.; Eriksson, G.; Hack, K.; Mahfoud, R.B.; Melançon, J.; Pelton, A.D.; Petersen, S. FactSage thermochemical software and databases. *Calphad* **2016**, *54*, 35–53. [[CrossRef](#)]
37. Yu, F.; Zhang, J.; Yang, Y.; Song, G. Reaction mechanism and electrochemical performance of LiFePO₄/C cathode materials synthesized by carbothermal method. *Electrochim. Acta* **2009**, *54*, 7389–7395. [[CrossRef](#)]
38. Xie, X.; Cheng, H. Adsorption and desorption of phenylarsonic acid compounds on metal oxide and hydroxide, and clay minerals. *Sci. Total Environ.* **2021**, *757*, 143765. [[CrossRef](#)] [[PubMed](#)]
39. Jie, Y.; Yang, S.; Li, Y.; Zhao, D.; Lai, Y.; Chen, Y. Oxidizing Roasting Behavior and Leaching Performance for the Recovery of Spent LiFePO₄ Batteries. *Minerals-Basel* **2020**, *10*, 949. [[CrossRef](#)]
40. Castro, L.; Dedryve'ere, R.; Khalifi, M.E.; Lippens, P.-E.; Bre'ger, J.; Tessier, C.; Gonbeau, D. The Spin-Polarized Electronic Structure of LiFePO₄ and FePO₄ Evidenced by in-Lab XPS. *J. Phys. Chem. C* **2010**, *114*, 17995–18000. [[CrossRef](#)]